Entanglements in Polymer Solutions under Elongational Flow: A Combined Study of Chain Stretching, Flow Velocimetry, and Elongational Viscosity

A. Chow,† A. Keller,* A. J. Müller, and J. A. Odell

H. H. Wills Physics Laboratory, University of Bristol, Tyndall Avenue, Bristol BS8 1TL, U.K. *Received November 17, 1986*

ABSTRACT: The progressive development of entanglements can be detected by observing strain patterns during increasing elongational strain rate where each stage is attributable to a transient network with a lifetime appropriate to the corresponding strain rate. The flow velocities are affected locally by transient network stretching, and this has pronounced influence on the macroscopic flow resistance (elongational viscosity). The latter should be highly relevant to the interpretation of continuum hydrodynamics of polymer solutions within elongational flow fields in terms of molecular behavior. The present work shows that this will only be possible by taking account of the "microstructure" in molecular strain and in the correspondingly modified flow velocities, arising as a consequence of the long relaxation times associated with the stretching of transient networks.

1. Introduction

This paper is concerned with entanglements in semidilute solutions, also with relevance to the flow modifying effect of polymeric additives. It is based on our new approach to the study of chain molecules relying upon the chain extending effect of elongational flow fields.[1] It has been shown previously that the extension of the chains in the entangled state is clearly distinct from that of the isolated chain in terms of the birefringent strain pattern as observed by our experimentation,[2] a distinction which provides a new method for registering entanglements.

More recent work has revealed that in a system of overlapping molecules the entanglements do not develop in a single stage on increasing strain rate as we reported previously,[2] but through an intriguing, yet characteristic sequence of stages. It is the reporting of this sequence, together with some associated flow modifications, leading to a qualitative appreciation of the principles involved, which will be the first objective of the paper.

As a further, and principal, objective we shall show how the strain patterns arising can be linked with the macroscopically registered flow behavior, thus creating a connection between deformation on the molecular level and macrorheology. The latter involves the measurement of macroscopic flow resistance, which has led to the design of a method for elongational viscometry in a totally fluid system—in contrast to available methods requiring self supporting threads. We also uncovered new signposts to flow-induced chain degradation.

The work here reported has been selected from an ever more diverse larger body of material, so as to enable us to convey, what we currently consider as the principal message. Admittedly confined to one technique, for creating elongational flow fields we believe that our conclusions are pertinent to inhomogeneous flow fields with persistently extensional components in general.

2. Principles and Method

An isolated flexible chain molecule undergoes a coil → stretch transition at a critical elongational strain rate, $\dot{\epsilon}_c$. This is a prediction from theoretical considerations[3] being due to hysteresis of molecular relaxation time with chain extension, where the critical strain rate is related to the relaxation time by

$$\dot{\epsilon}_c \tau \approx 1 \tag{1}$$

Extensional flow fields have been realized experimentally, and the criticality of the coil→stretch transition successfully corroborated.[1] τ is predicted from the theory of hydrodynamically screened solvated molecules to depend upon molecular weight as[4]

$$\tau \approx \eta_s M^\alpha / kT \tag{2}$$

where η_s is the solvent shear viscosity, M is the molecular weight, and α is an exponent expected to be in the range 1.5–1.8.

The elongational flow is created by various devices. Here we concentrate on the opposed jets (Figure 1a), by which a well-controlled uniaxial extensional flow field is created through sucking the solution simultaneously into both jets. By symmetry, the center of the jets is a stagnation point. The strain rate is calculated from a knowledge of the total fluid flow rate and the assumption of a uniform jet entrance velocity.[1,5] Thus the strain rate is related to the total flow rate (Q) as

$$\dot{\epsilon} = Q/2\pi r^2 d \tag{3}$$

where r is the jet radius and d the gap between the jets. Figure 1b shows the experimental flow field as visualised by light scattered at 90° from tracer particles.

The resulting chain elongation is monitored by the induced birefringence observed between crossed polars. In dilute solution elongation sets in abruptly at $\dot{\epsilon}_c$ as indicated by the appearance of a narrow birefringent line.

The extreme localization of the line arises from the requirement that the deformed molecule must accumulate a large *strain* before it becomes highly birefringent. Such strains can only be realized by fluid elements which pass sufficiently close to the stagnation point.[1] As will be seen, for mutually interacting chains this sharply defined zone of chain extension becomes delocalized in a specific manner.[2]

The polymers used were atactic polystyrene (a-PS) and polyethylene oxide (PEO). The a-PS was of high molecular weight (2.75×10^6 $\bar{M}_w$) and closely monodisperse ($\bar{M}_w/\bar{M}_n < 1.05$) (supplied by Polymer Laboratories Ltd). The a-PS was dissolved in Decalin, which has a viscosity of 0.002 75 Pa-s and is close to a Θ solvent at room temperature. This permitted quantitative deductions about relaxation times and overlap concentrations. The PEO sample used (supplied by BDH Ltd.) was of $\bar{M}_w > 5 \times 10^6$. Such polydisperse PEO is less suitable for quantitative assessment but proved convenient to display qualitatively the sequence of events involved. The PEO was dissolved in distilled water (η_s = 0.001 Pa-s). Water is regarded as a good solvent for PEO at room temperature (about 24 °C); however, the experimentally determined exponent α of 1.5 corresponds to a nonfree draining coil close to the Θ state;

† Present address: Stanford Research Institute, 333 Ravenswood Avenue, Menlo Park, CA 94025.

0024-9297/88/2221-0250$01.50/0

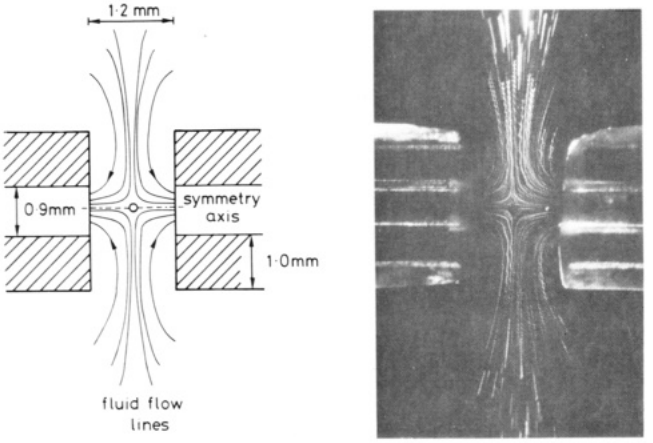

Figure 1. (a) Opposed jets. Polymer solution is sucked into the jets along the symmetry axis. The open circle represents the stagnation point in the center of the flow-field. (b) Flow field visualized by light scattered at 90° from tracer particles, (PEO solution corresponding to Figure 2a).

this apparent discrepancy has received some theoretical attention but is not completely resolved.[6,7]

3. Extending Entanglements

Two distinct stages in the development of birefringence with increasing strain rate for semidilute solutions have been identified previously:[2] The birefringence first appears as shown in Figure 2a. The line is almost indistinguishable from that in a dilute solution, corresponding to extension of individual chains beyond a critical strain rate. This phenomenon occurs for *all* concentrations examined so far (up to 3% in the case of PEO).

Above a limiting concentration (c^+_n) and at a much higher strain rate ($\dot{\epsilon}_n$), highly delocalized birefringence sets in abruptly (Figure 2 h). This birefringence extends upstream several millimeters beyond the entrance to the jets and is unstable, fluctuating rapidly with time. This effect we previously termed "flare" and attributed to mechanically effective molecular entanglements.[2] At the short time scale of $\tau_n = (1/\dot{\epsilon}_n)$ the chains no longer have sufficient time to disentangle before extending: the solution thus responds as a transient network and long-range orientation occurs. We interpreted τ_n as the effective disentanglement time of this network.

The postulation of the existence of a critical lower concentration is consistent with the concept of a network. As for a network to arise there needs to be a pathway of mutual contact across the whole macroscopic system, the establishment of which, as common with all such percolation problems, is a critical phenomenon. In our case the minimum contact criterion is clearly the existence of coil overlap.

The criterion of coil overlap is familiar in solution theory, where it represents the transition from dilute to semidilute solutions, the corresponding concentration being denoted as c^*. c^* is calculated on the basis that the chains can be represented as spheres of dimensions defined by the radius of gyration (R_g) and corresponds to the concentration at which contact between spheres is established. This criterion for c^* is calculated in slightly different ways by different authors.

c^+_n, the lower limit for the flare effect, was found to be at a concentration lower by a factor of 10–50 than the calculated c^*.[2] Without any further assumption this means that the elongational flow-induced extension registers a much lower degree of chain overlap than implied by the conventional c^* criterion for semidilute solutions. Or looking at it in another way, our methodology provides a considerably more sensitive test for chain overlap, hence entanglements, than the traditional criterion for semidilute solutions.

The reason for this is likely to reside in the fact that a single parameter, such as R_g, is inadequate for defining conditions for interchain contact, and the segment density in the overlap region as a function of center-to-center distance, which in turn is a function of concentration, needs considering instead. This characterizes the degree to which two coils in the θ state "see" each other. The effect is overlayed by any specific interactions between coils. In the simplest case it describes the opportunity for the formation of topological entanglements. Thus entanglement effects that show up on a macroscopic time scale are characterized by a high degree of interaction (e.g. neutron scattering,[8] viscometry). At short times the degree of interaction required for connectivity is much reduced since even tenuous entanglements on the periphery of the coils cannot disentangle quickly enough.[9]

Here in the new work we shall proceed to show that in the time scale between τ and τ_n a number of complex phenomena occur that reflect the systematic development of molecular connectedness.

Figure 2a–h illustrates a typical sequence of observations as the strain rate is increased. With increasing $\dot{\epsilon}$ a sharply localized line appears (Figure 2a) which progressively broadens (Figure 2b). Next a dark central line appears at $\dot{\epsilon}_p$ (Figure 2c) which itself broadens progressively (Figure 2d). For further increase in $\dot{\epsilon}$ a central narrow bright line reappears within the dark central zone (Figure 2e). Occasionally the new central line has been seen to split producing the appearance of four parallel bright lines (Figure 2f). These birefringent structures can develop up to the complete width of the capillary cross section. Following this the whole system becomes unstable and oscillates (Figure 2g) until the fully developed flare appears (Figure 2h).

Extensive observations reveal that the appearance of a dark central line corresponds to the onset of the formation of a birefringent "pipe" with a "hollow" (i.e. nonbirefringent) interior. This is deduced from the fact that the maximum retardation in our experiments is always much below one wavelength (λ). Consequently, the dark bands cannot be ascribed to retardation of the order of $n\lambda$, which is substantiated by their visibility also in white light as for Figure 15 in ref 1, without observation of interference colors. Relative darkening, therefore, corresponds to lowered retardation hence for a given birefringence to shorter path length, which will be the situation pertaining to the central axial regions when viewing a birefringent pipe. Further, recent observations of light scattered at 90° from the stretched molecules have also revealed a pipelike structure beyond $\dot{\epsilon}_p$ (see below).[10] This phenomenon has been previously ascribed in a-PS[11] to a change of sign of the birefringence with stretching due to free rotation of phenyl rings, an explanation no longer viable since the same phenomenon has been seen to occur in PEO (present work) and poly(acrylamide).[10,12]

Figure 3 provides a "phase diagram" for the appearance of the visually observed phenomena as a function of concentration and strain rate for PEO (5×10^6 $\bar{M}_w$). The following features are indicated: $\dot{\epsilon}_c$, $\dot{\epsilon}_p$ (first appearance of the pipe), and $\dot{\epsilon}_n$ (the flare) with $\dot{\epsilon}_c < \dot{\epsilon}_p < \dot{\epsilon}_n$.

Compared to $\dot{\epsilon}_p$ and $\dot{\epsilon}_n$, $\dot{\epsilon}_c$ decreases only slowly with c. As shown previously and confirmed by present work, this decrease is caused by the increase of solution viscosity[2] and

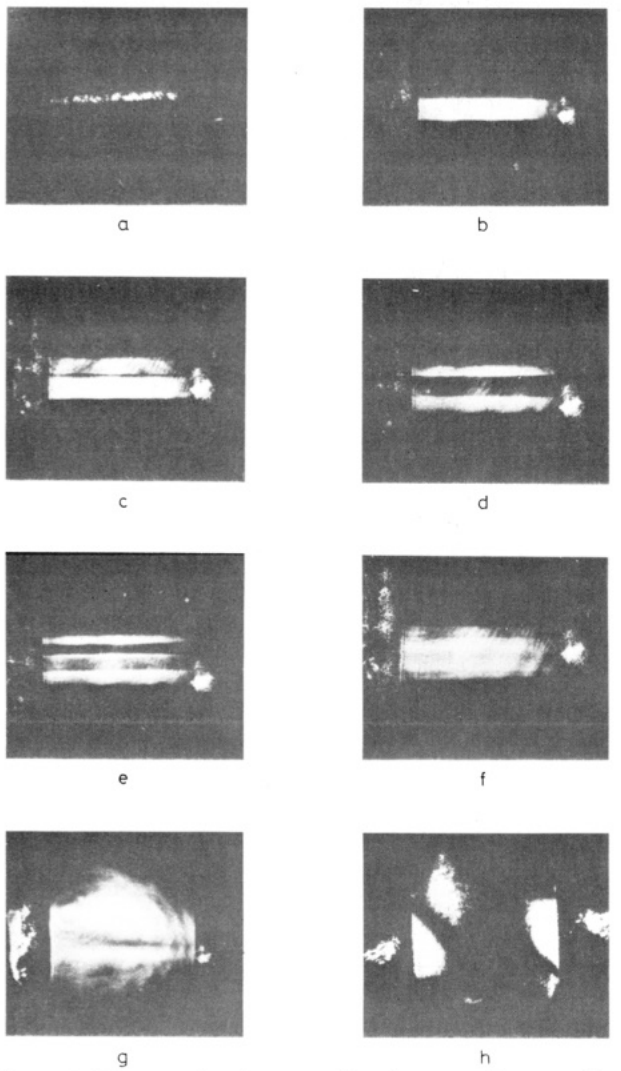

Figure 2. Photographs of stages of development of connectivity as the strain-rate is increased. The corresponding strain rates for a 0.2% solution of PEO ($\bar{M}_w > 5 \times 10^6$) in water are (a) 150 s^{-1}, (b) 200 s^{-1}, (c) 450 s^{-1}, (d) 500 s^{-1}, (e) 575 s^{-1}, (f) 650 s^{-1}, (g) 700 s^{-1}, and (h) 800 s^{-1}.

is well-accounted for by replacing η_s with solution viscosity in eq 2. Accordingly, the extending molecule is seeing the others merely a source of viscous drag. There is no limiting lower c: $\dot{\epsilon}_c$ extends to, and as supported by many other experiments down to concentrations of 2×10^{-5} levels off, at infinite dilution. In contrast, both $\dot{\epsilon}_p$ and $\dot{\epsilon}_n$ only set in at a certain concentration. First they decrease rapidly and then more slowly with c. The $\dot{\epsilon}_p$ vs c line is roughly parallel to $\dot{\epsilon}_n$ but is displaced to lower strain rates.

The low concentration cutoff signifies that both $\dot{\epsilon}_p$ and $\dot{\epsilon}_n$ are manifestations of the onset of molecular interactions. We will return to their interpretation in section 5.

The whole sequence shifts both to lower c and to lower $\dot{\epsilon}$ with increasing molecular weight. This follows from the established molecular weight dependence of $\dot{\epsilon}_c$[1] and from the expectation that longer chains will overlap at lower concentrations and that lower $\dot{\epsilon}$ are required to extend a more overlapping system. For a broad molecular weight distribution, as in the present PEO, it is the high molecular weight end which dominates the effects displayed; at any particular strain rate, only those molecules with sufficiently long relaxation times or which satisfy the overlap criterion will participate.

One can be more quantitative from the analogous experiments on the closely monodisperse a-PS. Figure 4

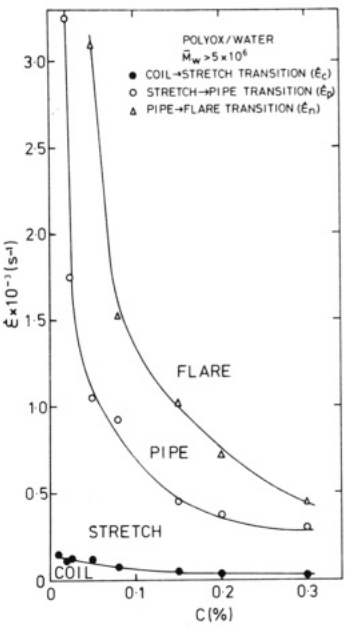

Figure 3. "Phase diagram" of the development of connectivity as a function of strain rate and concentration (PEO/water, $\bar{M}_w > 5 \times 10^6$).

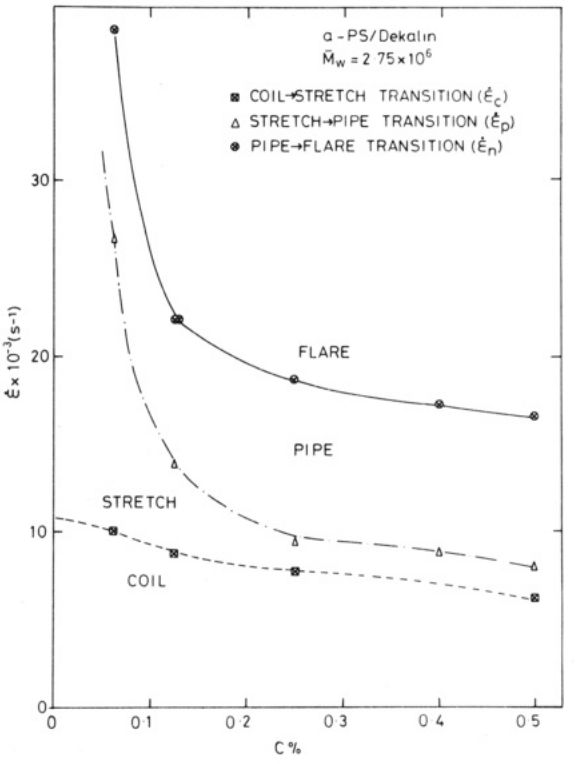

Figure 4. "Phase diagram" as in Figure 3 for a-PS, $\bar{M}_w = 2.75 \times 10^6$ in Decalin.

shows a "phase diagram" analogous to that of Figure 3, but for a-PS of $\bar{M}_w = 2.75 \times 10^6$ ($\bar{M}_w/\bar{M}_n < 1.05$). The overall behavior follows the same sequence with increasing strain rate and concentration as for PEO. The critical network overlap concentration (c_n^+) is of the order of 0.1% while that for incipient entanglement formation (c_p^+) could even be lower (see Figures 3 and 4). This means, as stated in the Introduction, that our elongational flow effects are sensitive to lower degrees of chain overlap or to network effects that are on a very short time scale, compared to the conventional c^* calculations (1–5%) and corresponding static experiments respectively.[2]

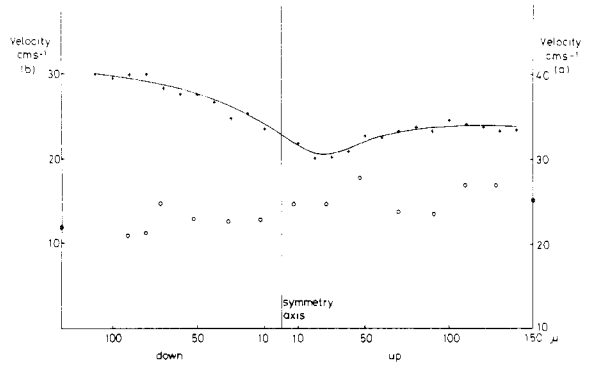

Figure 5. Velocimetry scans. Velocity as a function of position across the birefringent line: (a) open circles, dilute (0.03%); (b) crosses, semidilute solution (0.2%) (a-PS, $\bar{M}_w = 4 \times 10^6$ in Decalin).

The time scales, as expressed by τ_n, are of interest as they correspond to the appropriate disentanglement times. It has been remarked previously that τ_n is of the order of the time required for overlapping molecules to diffuse out of each others range as based on the statically measured diffusion coefficient.[2]

The "phase diagrams" of Figures 3 and 4 have a further notable feature. Although the curves for $\dot{\epsilon}_c$, $\dot{\epsilon}_p$, and $\dot{\epsilon}_n$ at first seem to converge with c, they do not cross, up to the highest concentrations examined. In the case of $\dot{\epsilon}_c$ this means that chains remain fully extendable as individuals provided they are being stretched on a long enough time scale to allow them to disentangle from the increasingly overlapping environment. Clearly, the issue of what the upper limiting concentration may be, or whether there is one at all, is of great potential interest for attempts to stretch out chains in the condensed phase.

4. Local Flow Velocities

The flow velocities have been determined as a function of position. Earlier works,[13-15] on the rectangular walled "cross-slot" device (which produces an approximately pure shear flow field), have shown that in dilute solution the localized chain extension has no effect on the local flow velocity profile. Nevertheless a sharp central decrease appeared in the velocity profile in the exit channel beyond a certain concentration. At that time this dip in velocity could not be correlated with features in the image of the strain field.

The real fringe photon-correlator velocimetry system presently used is capable of precise measurements of local velocity within a volume of about (10 μm).[3] Figure 5a shows the velocity profile scanning across a birefringent line of 30-μm width (i.e. above $\dot{\epsilon}_c$) in a dilute (0.03%) solution of a-PS ($\bar{M}_w = 4 \times 10^6$) in dekalin. The velocity distribution is not significantly different from that of pure solvent, corroborating that in sufficient dilution the extended molecules do not significantly perturb the flow field. Indeed, even in semidilute solutions the flow field is not significantly perturbed for $\dot{\epsilon} < \dot{\epsilon}_p$ below the appearance of the pipe. This is shown in a qualitative sense by the flow field illustrated in Figure 1b which corresponds to a 0.2% solution of 5×10^6 $\bar{M}_w$ PEO above the coil → stretch transition but below the pipe (corresponding to the birefringent line of Figure 2a). This flow field is indistinguishable from that of pure water. Figure 5b shows a similar scan but across a line of 100-μm width displaying a "pipe" birefringence obtained for a more concentrated solution (0.2%). The latter displays a clear "dip" in the velocity along the axis of the jet system where the dark line is seen in the image. This solution corresponds closely to the pipe region of the "phase diagram" shown in Figure 4. Visually the appearance is similar to Figure 2d for PEO.

The above result is quite general. It follows that the appearance of the pipe is associated with a corresponding local reduction in flow velocity, and conversely, that the extending chains produce observable flow modification only beyond the concentration (c_p^+) and strain rate ($\dot{\epsilon}_p$) where the pipe effect appears.

The result that the central dark line of the pipe is associated with a zone of lower flow velocity offers a ready explanation for the pipe effect. Namely, that the broadened chain extended regions "screen" the flow within, so that the flow velocity and hence the extensional strain rate, drops within the central zone. When $\dot{\epsilon}$ drops below criticality, $\dot{\epsilon}_c$, chain extension and consequent birefringence cease along the central axis giving rise to the effect observed.

5. Interpretation of Flow Patterns

Consider for simplicity a monodisperse system (the same should apply for a polydisperse one, but with reference to the range of molecular weights). At $\dot{\epsilon}_c$ the chains stretch out individually, yet the extension remains confined to those streamlines which pass close to the stagnation point ensuring sufficient residence time and hence molecular strain. It is important to note that the molecular strain can be much lower than the strain of a corresponding fluid element but increases toward this value at high strain rate.[16] As the strain rate is increased beyond $\dot{\epsilon}_c$, progressively higher molecular strains are attained also along outer streamlines corresponding to decreasing residence times, and the birefringent line broadens accordingly. The extending chains are expected to extract energy from the flow in the localized regions where the extension occurs, with a concomitant reduction in local flow velocity. It is to be expected further that such energy extraction will affect the flow increasingly toward the interior of the cylindrical extended-chain region, where molecular strains are highest. As the cylinder broadens, the flow velocity should be progressively reduced along the central axis, the result given by our flow velocimetry. Once it falls below that corresponding to the critical strain rate $\dot{\epsilon}_c$, the chains will cease to become extended there, from which the central dark line and hence and hollow pipe effect follows.

Any flow modifying effect will be larger for higher concentration, where there are more molecules to extend per unit volume even without considering molecular interaction. As already stated, the fluid strain diminishes when passing from central axis to periphery; this will limit the chain extension and hence the birefringent line width that can be attained. However, for the transient network that arises beyond c_p^+, much less strain is required for full orientation than for isolated molecules. It follows that network chain extension will spread out to more peripheral stream lines than encompassed by the original birefringent line. This coupled with the higher concentration leads to a correspondingly increased screening of the flow along the central axis, setting off the sequence of effects under consideration.

The broadening of the pipe for $\dot{\epsilon}$ beyond $\dot{\epsilon}_p$ would clearly follow from the above considerations. Indeed, on the basis of a semiempirical model of the opposed jet flow field[16] the outermost pipe diameter (~300 μm) corresponds to a fluid strain of the order of only 10×, such low strains would not produce appreciable birefringence for isolated molecules; only deformation of a network would give significant molecular orientation. However, as the screening of the pipe interior is not expected to be complete, the velocity will also rise there on further increase of the mean $\dot{\epsilon}$. It is readily visualized that the central strain rate could

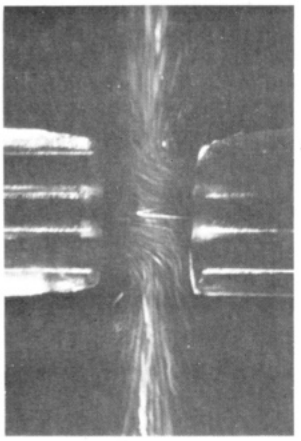

Figure 6. Flow field visualized by light scattered at 90° from tracer particles during fully developed flare (corresponding to Figure 2h).

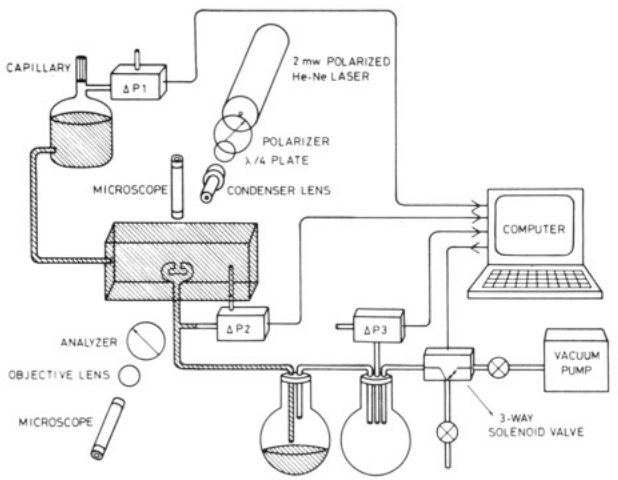

Figure 7. Schematic diagram of the apparatus for measurement of extensional birefringence and flow resistance.

reattain the value $\dot{\epsilon}_c$ when a new localized central birefringent line should arise, as in fact observed (Figure 2e).

During the above process of pipe development it seems that the network behavior itself remains highly localized; this enables the fluid as a *whole* to conform with the convergent flow field. At higher strain rates, corresponding to τ_n, the whole region becomes a transient network (because of the very short time scale of deformation). Affine deformation of such a network is inconsistent with an extensional flow field incorporating a stagnation point (and hence infinite strains). Consequently, the cylindrically symmetric nature of the flow field breaks down completely,[10] the result being the generalized birefringence and marked flow instability observed. The flow lines in flare are shown in Figure 6 as revealed by light scattered at 90° from tracer particles. While the stream lines observed clearly show a flow instability, this is not associated with inertial turbulence, since the Reynolds number is aproximately 1000, calculated on the basis of Poiseuille flow in the jets, and turbulence can be identified in pure solvent at 2888 s^{-1}, i.e. Reynolds number 3087. The supposition that no turbulence occurs in strongly supported by subsequent viscometry data (Figure 8).

6. Flow Resistance–Elongational Viscosity

It is to be expected that the dramatic effects associated with the formation of transient networks will also have a correspondingly pronounced influence on the macroscopic flow behavior and, in particular, that the visually observed

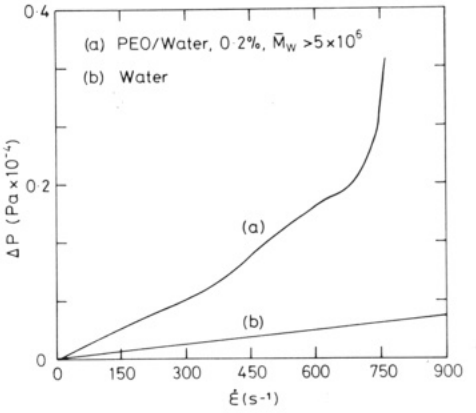

Figure 8. Pressure drop across the jets ΔP_2 versus $\dot{\epsilon}$ (Bernoulli corrected curves): (a) semidilute PEO and (b) water.

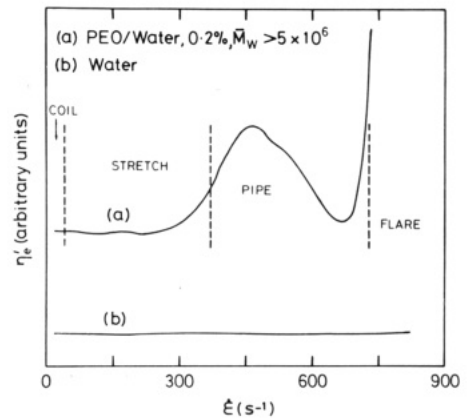

Figure 9. η_e' versus $\dot{\epsilon}$ curves derived from Figure 8; (a) semidilute PEO, indicating the characteristic flow behavior as in Figure 3, and (b) water.

events are reflected by changes in the flow resistance presented by the jet system as a whole.

In order to quantify flow resistance, we have measured the pressure drop across the jets (ΔP_2) as the strain rate $\dot{\epsilon}$ is increased. Figure 7 shows a schematic diagram of the apparatus used to control strain rate, observe birefringence, and monitor the pressure drop across the jets. The total flow rate (Q) is derived from the pressure drop due to air flowing into the solution reservoir through a capillary (ΔP_1), and the use of eq 3 enables strain rates to be derived. This is monitored by the computer which controls the suction applied to the jets (ΔP_3) through a solenoid valve in order to uniformly increase the strain rate, as the pressure drop across the jets (ΔP_2) is recorded. The illumination is provided by a 2-mW polarized He–Ne laser and the birefringence patterns observed between crossed polars utilizing a $\lambda/4$ plate as a Senarmont compensator.[10] The ΔP vs $\dot{\epsilon}$ traces thus obtained showed a curvature even with pure solvent which originated from the Bernoulli effect due to convergent flow, an effect which could then be corrected for analytically. Figure 8 shows such a corrected trace. The slope of the corrected ΔP_2 vs $\dot{\epsilon}$ curve ($d(\Delta P_2)/d\dot{\epsilon}$) then provides a quantity proportional to an elongational viscosity η_e. We shall define ($d(\Delta P_2)/d\dot{\epsilon}$) as an effective elongational viscosity η_e', a quantity we shall use for displaying some of the results in what follows. This measure of extensional viscosity is a well-defined function of macroscopic strain rate, but, because of the presence of the stagnation point, it must correspond to a combination of a wide range of fluid strains. Because of the way ΔP_2 is measured, there will also be a contribution to η_e' from Poiseuille flow inside the jets. Thus due to the spatial

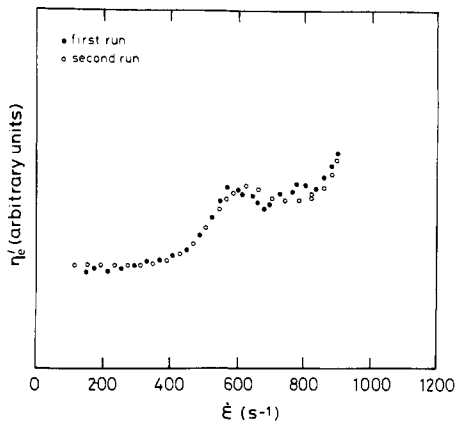

Figure 10. η_e' versus $\dot{\epsilon}$ for two successive runs of a 0.2% PEO/water solution ($\bar{M}_w > 5 \times 10^6$) where the experiment was stopped below $\dot{\epsilon}_n$.

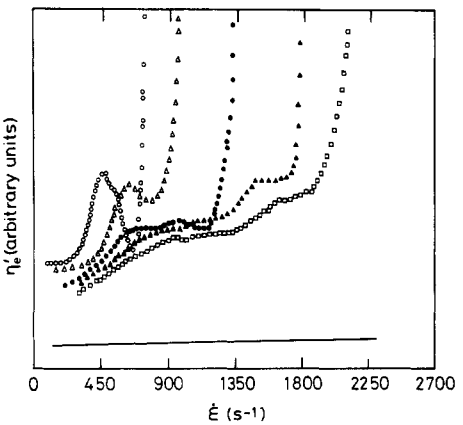

Figure 11. η_e' versus $\dot{\epsilon}$ for successive runs of a 0.2% PEO/water solution ($\bar{M}_w > 5 \times 10^6$) where each run extends beyond $\dot{\epsilon}_n$: ○, first run; △, second run; ●, third run; ▲, fourth run; □, fifth run; solid line, pure water.

variation of strain and strain rate, it is important not to regard η_e' as a true elongational viscosity.

Figure 9 shows η_e' as a function of $\dot{\epsilon}$. The initial constant value corresponds to a pseudo-Newtonian viscosity. At the point at which the pipe is formed there is a pronounced peak, in the present case at $\dot{\epsilon} = 465\ s^{-1}$. At still higher $\dot{\epsilon}$, when the birefringence flares, the flow becomes irregular with the extensional viscosity enormously increased (only the initial portion of the rise is shown). The reality of all these effects is borne out by comparison with the totally invariant η_e' value for the pure solvent (water) recorded under otherwise identical circumstances. Closer inspection of Figure 9 reveals further details. Thus, there is a shoulder on the high end of the peak associated with the pipe effect. Other traces may in fact show a double (Figure 10) or even a triple peak (some traces in Figure 11) within the pipe effect region. By all indications these periodicities in the η_e' vs $\dot{\epsilon}$ curves correspond to the periodic sequences in the visual image of pipe development described previously.

In summary, we thus have a correspondence between the visually registered development of transient entanglement formation and the macroscopic flow characteristics. Accordingly, entanglement formation is associated with an increase in flow resistance and in η_e' derived therefrom, leading to a massive increase when the network becomes infinite as signalled by the flare. The overall direction of the effect, i.e. an increase in η_e' with $\dot{\epsilon}$, might have been anticipated. However, the minima in η_e' with increasing $\dot{\epsilon}$ are unexpected. Nevertheless, even these effects seem to fall into a consistent scheme in the light of the sequence of visual images observed. The fall in η_e' corresponds closely to the transition from a broadened line to a pipe of initially similar diameter. The pipe, therefore, corresponds to fewer birefringent (i.e. stretched) molecules in the flow field, presenting a lower net resistance to the extensional flow.

These findings have wider implications for the study of inhomogeneous but still laminar flows. Namely, any macroscopically measured flow parameter can only be an aggregate expression of the wide spatial variations within the flow field resulting from inhomogeneities in molecular strain. Conversely, it follows that molecular behavior cannot be extracted from macroscopic flow measurements alone without local probing of the "morphology" of both strain and flow fields.

A further important aspect emerges from the reversibility characteristics of the curves such as in Figures 10 and 11. The ΔP_2 (and the derived η_e' vs $\dot{\epsilon}$) plots are almost reproducible for reruns up to the onset of flare, including the pipe effect (Figure 10). However, once the flare stage has been reached, the same plots for subsequent consecutive reruns show a reduction in the initial value of η_e', and the flare and associated effects are shifted to higher strain rates (Figure 11). These effects are consistent with a progressive reduction in molecular weight as chains are broken by stretching beyond $\dot{\epsilon}_n$. Such chain scission is confirmed by GPC molecular weight measurements which show a progressive destruction of the high molecular weight tail. Clearly, as discussed in section 5, deformation of such a network is inconsistent with an extensional flow field incorporating a stagnation point: the consequences are molecular scission and flow modification (annihilation of the stagnation point).

We thus see that in addition to its intrinsic significance the rheological behavior provides strong additional support for our picture of network formation, in particular the interpretation of the flare effect. Further, and rather unexpectedly, it conveys information on flow-induced chain scission. We have now identified two kinds of flow-induced degradation. First, the isolated chain, when stretched out breaks virtually exactly in the center yielding two closely equal chain halves as the elongational flow rate is increased far enough beyond the coil → stretch transition.[11,17] The second mode of scission, as reported here, applies to overlapping chains which break during the flare stage. Although not yet fully confirmed, here fracture is not expected to be closely central to the molecule. While both fracture modes can occur, the second, involving entanglements, takes place at lower strain rates.

7. Conclusion

The observed effects demonstrate the progressive development of the entanglements beyond a critical overlap concentration, as a function of strain rate. This is attributable to the activation of transient mechanical connectedness at the appropriately decreasing time scale coupled with localized flow modifications produced thereby. The associated rheological effects reveal the intricate relation between macroscopic flow parameters and molecular behavior even in laminar elongational flows. Any macroscopically measured flow parameter can only be an aggregate expression of the wide spatial variations within the flow field resulting from inhomogeneities in molecular strain. Conversely, molecular behavior cannot be extracted from macroscopic flow measurements alone without local probing of the "morphology" of both strain and flow fields. This work should provide new pointers for understanding fluid transport with polymeric additives

and a new approach to the study of entanglements and flow-induced chain scission.

Acknowledgment. We are pleased to acknowledge the support of the Venture Research Unit of BP International during the course of this research.

Registry No. a-PS, 9003-53-6; PEO, 25322-68-3.

References and Notes

(1) Keller, A.; Odell, J. A. *Colloid Polym. Sci.* **1985**, *263*, 181.
(2) Odell, J. A.; Keller, A.; and Miles, M. J. *Polymer* **1985**, *26*, 1219.
(3) de Gennes, P.-G. *J. Chem. Phys.* **1974**, *60*, 5030.
(4) Zimm, B. H. *J. Chem. Phys.* **1956**, *24*, 269.
(5) Frank, F. C.; Keller, A.; Mackley, M. R. *Polymer* **1971**, *12*, 467.
(6) Rabin, Y. *J. Polym. Sci., Polym. Lett. Ed.* **1985**, *23*, 11.
(7) Rabin, Y.; Henyey, F. S.; Pathria, R. K. *Phys. Rev. Lett.* **1985**, *55*, 201.
(8) Cotton, J. P.; Nierlich, M.; Bove, F.; Daoud, M.; Farnoux, B.; Janninck, G.; Dupplesix, R.; Picot, C. J. *J. Chem. Phys.* **1976**, *65*, 1101.
(9) Keller, A.; Müller, A. J.; Odell, J. A. *Progr. Colloid Polym. Sci.*, in press.
(10) Odell, J. A.; Müller, A. J.; Keller, A., submitted for publication in *Polymer*.
(11) Odell, J. A.; Keller, A. *J. Polym. Sci., Polym. Phys. Ed.* **1986**, *24*, 1889.
(12) Farinato, R. S. Abstract and Lecture, Bristol Conference Flexibility of Macromolecules in solution; Institute of Physics: London, England, 1986.
(13) Gardner, A.; Pike, E. R.; Miles, M. J.; Keller, A.; Tanaka, K. *Polymer* **1982**, *23*, 1435.
(14) Lyazid, A., Scrivener, O., Teitgen, R. In *Rheology*; Astarita, G., Marruci, G., Nicolais, L., Eds.; Plenum: New York, 1980; Vol. 2, p 141.
(15) Rabin, Y.; Henyey, F. S.; Creamer, D. B. *J. Chem. Phys.* **1986**, *85*, 4696.
(16) Odell, J. A. *J. Polym. Sci., Polym. Phys. Ed.*, in press.
(17) Odell, J. A.; Keller, A.; Miles, M. J. *Polym. Commun.* **1983**, *24*, 7.

Stress Relaxation and Chemical Kinetics in Pairwise Associating Polymers

M. E. Cates

Institute for Theoretical Physics, University of California, Santa Barbara, California 93106.
Received June 2, 1987

ABSTRACT: Within the framework of the tube model, a theoretical study is made of the dynamics of a concentrated system of long flexible macromolecules, each of which has a single functional end group that can associate with another such group to make a dimer. When the dissociation time of the dimer (τ_{break}) is very large compared with T_d, the disengagement time of an undimerized chain (or "monomer"), the zero-shear viscosity of the system approaches $\eta = (16q + 1)\eta_0/(2q + 1)$, with η_0 the viscosity of pure monomers and q the equilibrium ratio of dimers to monomers. In the opposite limit ($\tau_{break}/T_d \equiv \alpha \to 0$), the viscosity tends to $\eta = (2q + 1)\eta_0/(q + 1)$. For intermediate α (roughly $0.02 < \alpha < 50$), η depends quite sensitively on α and q; the relevant behavior is studied numerically. The results may be useful in obtaining estimates of the dissociation rate from measurements of the static equilibrium constant and the zero-shear viscosity.

Introduction

In recent years, there has been growing experimental and theoretical interest in associating polymers.[1-9] These are flexible chain molecules each containing one or more functional groups, which can form transient associations with one another. Such polymers frequently exhibit striking rheological behavior, such as shear thickening; they are of increasing technological importance as flow-modifying additives.[2-4] To be able to make best use of these materials, it is important to try to understand the relationship between the kinetics of association and dissociation and macroscopic flow properties. Conversely, one would like to be able to use rheological measurements on simple systems to obtain information concerning the underlying reaction kinetics.

Perhaps the simplest case of interest is when (i) the associating groups have a strong dimerizing interaction, such as occurs between carboxylic acid groups in a nonpolar solvent, and (ii) there is exactly one associating group, at one end, of every chain. In this case, there is a dynamic equilibrium between unassociated chains ("monomers") and 2-fold associates ("dimers"). Clearly, one expects the viscosity of the system to be higher than that of the unfunctionalized monomer. As emphasized by Worsfold and Bywater,[6] however, the magnitude of this viscosity enhancement can depend not only on the equilibrium constant for the dimerization but also on the reaction kinetics. These become relevant if the dissociation rate is high enough that significant rearrangement of the associations occurs on the characteristic time scale of stress relaxation (the terminal time).

In the present work, we assume that the equilibrium constant, or (equivalently) the ratio q of the equilibrium number densities of dimers to monomers, is known:

$$q \equiv [\text{dimer}]/[\text{monomer}] \quad (1)$$

We then study theoretically the stress relaxation behavior as a function of the reaction rate for dissociation. We will assume throughout that the chains are long enough (and the concentration high enough) to be always in the strongly entangled regime, in which the viscosity is a rapidly increasing function of chain length. In this regime, the dynamics of stress relaxation in the absence of functional groups is understood semi-quantitatively in terms of the tube model;[10,11] it only remains to incorporate the effects of the associations. Earlier work by the author has focused on extending the tube model to the case of "living polymers"—chains which can break reversibly at any point in the chemical sequence.[12,13] The physics in the present case is rather different, since breakage of a dimer is only possible at the midpoint; nonetheless, several of the basic ideas can be taken over, with a minimum of modification, from ref 12.

Reptation

In the tube model,[10,11] the dominant stress-relaxation pathway for an entangled polymer system is presumed to

0024-9297/88/2221-0256$01.50/0